Pulse accumulation, radial heat conduction, and anisotropic thermal conductivity in pump-probe transient thermoreflectance

Aaron J. Schmidt,[a] Xiaoyuan Chen, and Gang Chen
Department of Mechanical Engineering, Massachusetts Institute of Technology, Cambridge, Massachusetts 02139–4307, USA

(Received 27 June 2008; accepted 6 October 2008; published online 11 November 2008)

The relationship between pulse accumulation and radial heat conduction in pump-probe transient thermoreflectance (TTR) is explored. The results illustrate how pulse accumulation allows TTR to probe two thermal length scales simultaneously. In addition, the conditions under which radial transport effects are important are described. An analytical solution for anisotropic heat flow in layered structures is given, and a method for measuring both cross-plane and in-plane thermal conductivities of thermally anisotropic thin films is described. As verification, the technique is used to extract the cross-plane and in-plane thermal conductivities of highly ordered pyrolytic graphite. Results are found to be in good agreement with literature values. © *2008 American Institute of Physics.* [DOI: 10.1063/1.3006335]

I. INTRODUCTION

Pump-probe transient thermoreflectance (TTR) has been widely used to study thermal transport in thin films and bulk materials,[1–4] liquids,[5] and across material interfaces.[6,7] All of these experiments are variations of the optical pump-probe technique, in which a pump pulse is used to excite the sample, changing the optical properties, and a second time-delayed probe pulse measures the change. The change is subsequently correlated with a physical property of interest, usually through the thermoreflectance coefficient of a thin top layer of metal. The fine temporal resolution of the technique makes it well suited to the study of a wide range of transport processes occurring on time scales from femtoseconds to nanoseconds and longer. Typically, the data are compared to a model of the system, and the unknown physical properties of interest are adjusted to minimize the error between the model and the data.

A popular implementation of TTR has been to use a high repetition-rate pulse source such as the fundamental output of a Ti:sapphire laser oscillator, which typically has a pulsing frequency on the order of 80 MHz. For thermal measurement, this approach has significant advantages over lower repetition-rate amplified systems: in addition to being significantly simpler and less expensive, the high repetition rate allows for pump-beam modulation and lock-in detection at high frequencies, where laser power fluctuations can be reduced to the order of $10^{-7}/\sqrt{\text{Hz}}$,[8] and the relatively weak pulse energies limit temperature excursions of the sample to a few kelvins.[2] However, at high repetition rates, for many situations there is no sufficient time for the system to return to equilibrium between laser pulses. In this case, the effects of multiple pulses accumulate, and the measured signal will differ from the response to a single pulse. As we will see, the majority of thermal conductivity measurements fall into this category.

Several treatments of accumulating photothermal pulses have been given in the past for various techniques. A one-dimensional analysis was given in the context of photothermal rate-window spectrometry.[9] Accumulation phenomena were first described in the context of TTR by Capinski and Maris[10] in terms of the impulse response of the sample assuming one-dimensional thermal transport, and subsequently expressed in terms of the frequency response by Cahill[11] to account for radial heat conduction in layered isotropic media.

What is not obvious is why radial transport effects are important. In ultrafast pump-probe measurements, the time required for the response to an essentially instantaneous heat pulse to decay to a negligible value yields a thermal penetration depth that is much smaller than the laser spot size, and it is commonly assumed that one-dimensional transport is an adequate model.[1,2] In work where radial effects are considered, a different criterion for one-dimensional transport is suggested: the penetration depth of the thermal waves at the modulation frequency should be much smaller than the laser spot size[7,11] since the lowest frequency component of the thermal response that contributes to the signal is the modulation frequency of the pump beam. However, it is not immediately clear how radial effects enter into the solution or which thermal length scale dominates under a given set of experimental conditions.

In this work, we show explicitly how it is pulse accumulation that leads to radial transport effects and describe the conditions under which radial transport is important. We will see that although pulse accumulation complicates the analysis, it also makes TTR more powerful by allowing two length scales to be probed simultaneously.

In addition, an analytical solution for heat flow in layered media is given to account for anisotropic thermal conductivity, which is frequently encountered in natural and

[a]Electronic mail: aarons@mit.edu.

man-made thin film and bulk materials. We show how, by varying the modulation frequency and laser spot size in a TTR measurement, both in-plane and cross-plane thermal conductivities can be isolated. Using a two-color implementation,[5] the technique is applied to highly ordered pyrolytic graphite (HOPG), a well-known thermally anisotropic material. Results are in good agreement with literature values.

II. PULSE ACCUMULATION AND THE FREQUENCY RESPONSE

Various implementations of high-repetition rate TTR systems are described in literature.[3,5,10,12] Although the specific details of implementation vary, the essential elements do not. From an analysis point of view, there are three key features: (1) the laser emits a train of ultrashort pulses that are sufficiently short compared to the measurement time scale and pulse repetition period to be considered Dirac delta functions; (2) the laser output is split into two trains which are then separated in time by an adjustable delay, τ; and (3) the pump beam is modulated at a reference frequency, ω_0, and lock-in detection is used to extract only the components of the measured signal in an extremely narrow band around the reference signal.

It is assumed that the response of the sample to the laser input is both linear and time invariant (LTI). This assumption greatly simplifies analysis since we can use all the mathematical tools available for LTI systems, such as superposition, convolution, and simple conversion between the time the frequency domains. In conduction heat transfer, if the temperature changes are small enough that physical properties can be assumed constant, then the temperature of the system obeys superposition.[13] In addition, the thermoreflectance coefficient must be linear with temperature over the range of temperatures induced in experiment. Under typical experimental conditions, both the temperature rise due to a single pulse[2] and the steady state accumulation of heat[11] will be on the order of a few kelvins or smaller, so linearity should hold. The assumption is easily checked by changing the input power and by verifying that the measured signal scales correctly and does not change shape.

For clarity, the measurement process is depicted graphically in Figs. 1 and 2. Figure 1(a) shows the pump beam as a train of delta functions at the pulsing frequency of the laser. The time between pulses, T, is typically on the order of 12.5 ns. The pump beam passes through a modulator, usually an electro-optic modulator (EOM) or acousto-optic modulator, which chops the beam with a square wave modulation at the reference frequency, ω_0 [Fig. 1(b)]. Because lock-in detection is used, ideally the response to both the dc offset and the higher harmonics will be rejected, and we need only consider the fundamental modulation component at ω_0, shown in Fig. 1(c). If the lock-in amplifier mixes the signal with a square wave instead of a pure sinusoid, a resonant filter between the photodiode and the lock-in amplifier can be used to effectively remove the higher harmonic components.[8]

The thermal response of the sample is given by the convolution between the thermal response to a single heat pulse (the impulse response) and the modulated pulse train. Because, as we discussed in the preceding paragraph, the lock-in effectively removes any dc offset and higher harmonics, we can convolve the impulse response with the fundamental harmonic component of the EOM with no offset [Fig. 2(a)]. Neglecting all other frequencies gives the appearance that some of the heat pulses have a negative contribution; if all frequencies were included, then the sample temperature would increase during the period when the EOM allows pulses through and decrease when the pulses are blocked.[2] The probe pulses arrive at the sample delayed from the pump pulses by the delay time, τ, and are reflected into the detector with an intensity proportional to the surface temperature of the sample [Fig. 2(c)].

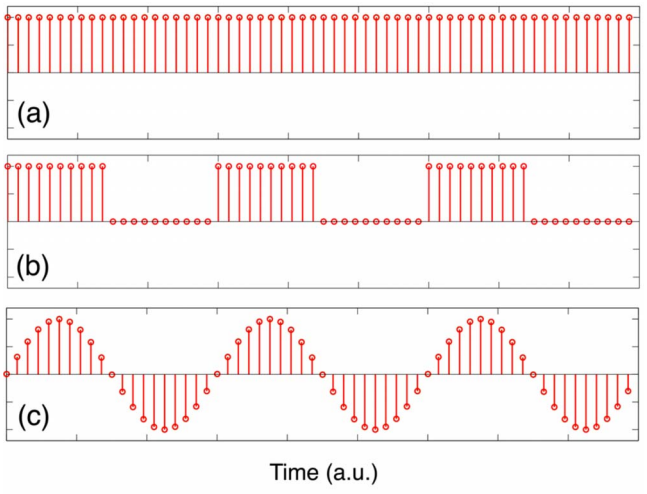

FIG. 1. (Color online) (a) The unmodulated pump beam represented as a train of delta functions with an angular frequency of $2\pi/T$. (b) The pump beam after passing through an EOM. (c) Modulation due only the fundamental harmonic component of the EOM.

Although the probe pulses also heat the sample and can in general be as strong or stronger than the pump pulses, this effect is not shown in Figs. 2(c) and 2(d) and can usually be ignored. This is because the probe beam is unmodulated. The time-domain representation of the probe beam is

$$p(t) = Q_{\text{probe}} \sum_{n=-\infty}^{\infty} \delta(t - nT - \tau), \tag{1}$$

which has the Fourier transform,[14]

$$P(\omega) = Q_{\text{probe}} \left[\omega_s \sum_{k=-\infty}^{\infty} \delta(\omega - k\omega_s) \right] e^{-i\omega\tau}. \tag{2}$$

Here δ is the Dirac delta function, T is the period between pulses, τ is the delay time between pump and probe pulses, Q_{probe} is the energy per probe pulse, and $\omega_s \equiv 2\pi/T$. Equation (2) evaluates to zero for all frequencies except multiples of ω_s. In our experiments, ω_s (80 MHz) is one to two orders of magnitude larger than the modulation frequency (1–10 MHz). We typically use a lock-in time constant of 30 ms, which gives a pass band of roughly 10 Hz.[15] Therefore, all of the probe frequencies will be well outside the lock-in pass band, and we can safely ignore the probe pulses' effect on the measurement and view them as simply measuring the state of the thermal system at a time τ after the pump pulses.

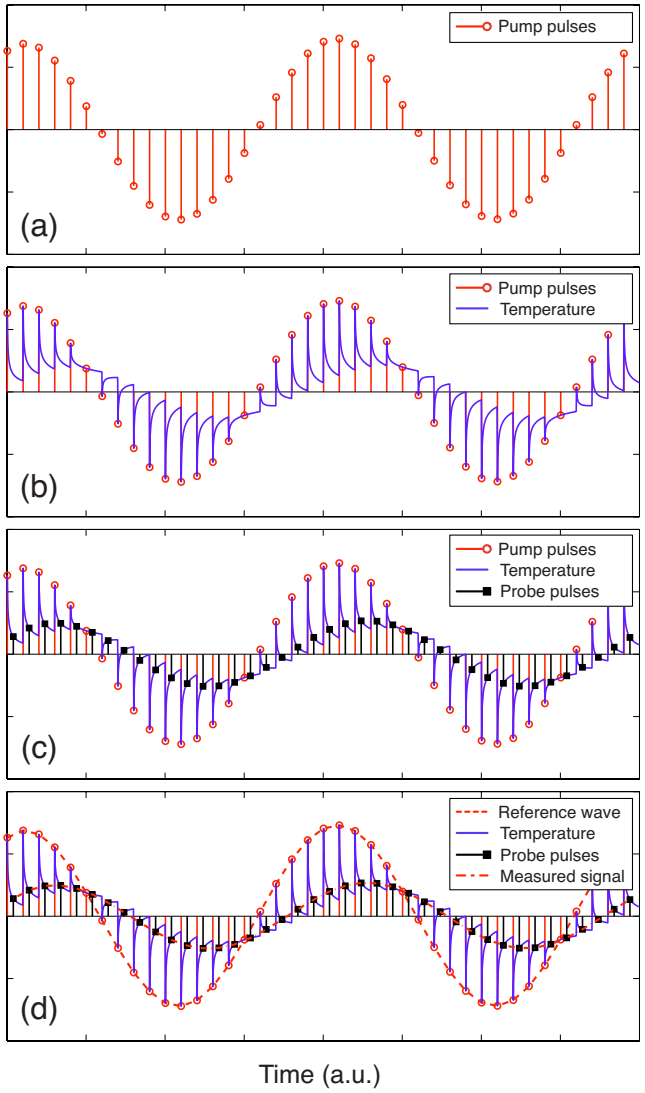

FIG. 2. (Color online) (a) The pump beam input to the sample modulated by the fundamental component of the EOM. (b) The surface temperature of the sample in response to the pump input. (c) The probe pulses arrive at the sample delayed by a time, τ, and are reflected back to a detector with an intensity proportional to the surface temperature. (d) The fundamental harmonic components of the reference wave and measured probe wave. The amplitude and phase difference between these two waves is recorded by the lock-in amplifier at every delay time.

The lock-in amplifier measures the fundamental component of the probe signal at the modulation frequency, ω_0, and rejects all other harmonic components. This is shown in Fig. 2(d). The output will be the amplitude, A, and phase, ϕ, of the fundamental component of the probe signal with respect to the reference wave at every delay time τ. Mathematically, the solution takes the form of a "transfer function," a complex number $Z(\omega_0)$ such that the output of the lock-in amplifier for a reference wave $e^{i\omega_0 t}$ is given by

$$Ae^{i(\omega_0 t+\phi)} = Z(\omega_0)e^{i\omega_0 t}. \tag{3}$$

The transfer function can be represented in two ways. The first, given by Capinski and Maris[10] is in terms of the impulse response of the sample, $h(t)$,

$$Z(\omega_0) = \frac{\beta Q Q_{\text{probe}}}{T}\sum_{q=0}^{\infty} h(qT+\tau)e^{-i\omega_0(qT+\tau)}, \tag{4}$$

where Q is the power per pump pulse, Q_{probe} is the power per probe pulse, and β is a constant that includes the thermoreflectance coefficient and gain of the electronics. A mathematically equivalent form was later given by Cahill[11] in terms of the sample frequency response, $H(\omega)$,

$$Z(\omega_0) = \frac{\beta Q Q_{\text{probe}}}{T^2}\sum_{k=-\infty}^{\infty} H(\omega_0 + k\omega_s)e^{ik\omega_s\tau}, \tag{5}$$

where again ω_0 is the reference frequency and $\omega_s \equiv 2\pi/T$. The equivalence of Eqs. (4) and (5) stems from the fact that, in a LTI system, the impulse response and frequency response are Fourier transform pairs. In practice, Eq. (4) may be more convenient for numerical simulations, while Eq. (5) is more convenient for cases where an analytical heat transfer solution is more easily obtained in the frequency domain.

In the limit that the time between pulses, T, becomes infinite, both expressions reduce to the impulse response as a function of delay time, τ,

$$\lim_{T\to\infty}\frac{\beta Q Q_{\text{probe}}}{T}\sum_{q=0}^{\infty} e^{-i\omega_0\tau}h(qT+\tau) = \frac{\beta Q Q_{\text{probe}}}{T}h(\tau)e^{-i\omega_0\tau} \tag{6}$$

since at very long times, $h(qT+\tau)$ decays to zero for all terms where $q \neq 0$. In this limiting case, the phase shift is simply the delay between the pump and probe pulses divided by the modulation frequency, as expected, and the amplitude of the signal can be directly interpreted as the response of the sample to a single pulse. In this case, the relevant time and length scales are those associated with the single-pulse response.

In the other limit, as T approaches zero, the expression approaches the frequency response (i.e., the steady periodic response at ω_0),

$$\lim_{T\to 0}\frac{\beta Q Q_{\text{probe}}}{T^2}\sum_{q=0}^{\infty} e^{-i\omega_0\tau}h(qT+\tau)T = \frac{\beta Q Q_{\text{probe}}}{T^2}H(\omega_0). \tag{7}$$

In this case, the relevant time and length scales are those associated with the steady periodic response.

In the intermediate range, where the decay time of the system is not much longer or shorter than the pulse period T, the signal has elements of both the impulse response and the steady frequency response and the two effects cannot be easily separated.

To examine this further, we take a simple exponential system as a model and see how the measured signal changes as the decay rate and laser pulse period are varied. Although the thermal response of a sample is more complex, the basic features of the accumulation effects will be the same. The impulse response and frequency response of the simple system are given by

$$h(t) = e^{-at}, \tag{8}$$

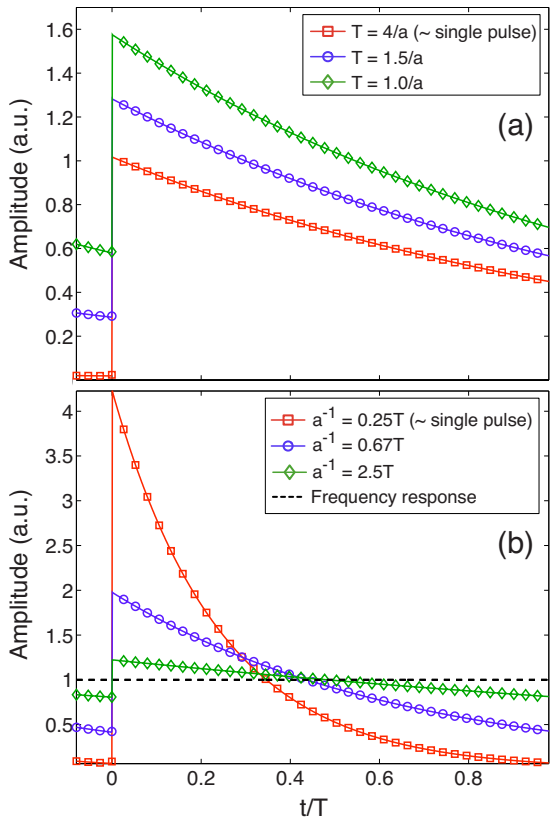

FIG. 3. (Color online) (a) The amplitude signal returned by the lock-in for a sample with an exponential response $h(t)=e^{-at}$ for three different pulse periods: $T=4/a$, $T=1.5/a$, and $T=1/a$. Results are plotted as a function of time T. (b) The pulse period T is fixed and the exponential decay time, $1/a$, is varied from $T/4$ to $2.5T$. Amplitudes are normalized to the amplitude of the steady periodic response, $|H(\omega_0)|$.

$$H(\omega) = \frac{1}{a + i\omega}, \tag{9}$$

where a^{-1} is the exponential decay time constant.

Figure 3(a) plots the amplitude of Eq. (5), $|Z(\omega_0)|$, using a fixed exponential decay time for three different pulse periods: $T=4/a$, $1.5/a$, and $1/a$. When the pulse period is $\sim 4/a$ or greater, $|Z(\omega_0)|$ is essentially the single-pulse response. As the decay time approaches the pulse period, the baseline signal for $\tau<0$ begins to shift upward and the shape of the signal changes: if the baseline is subtracted and the signals are normalized at a common time point, the signals where $T \to 1/a$ appear to decay faster. This can potentially lead to incorrect interpretation of the results, such as thermal conductivity value that is too large.

Figure 3(b) illustrates the accumulation effects from a different perspective. The pulse period, T, is fixed and the exponential decay time is varied from $a^{-1}=T/4$ to $a^{-1}=2.5T$. The amplitude signal $|Z(\omega_0)|$ is shown, normalized to the amplitude of the steady periodic response, $|H(\omega_0)|$. At $a^{-1}=T/4$, the response has zero baseline and is identical to the single-pulse response, but by the time $a^{-1}=2.5T$ the response is converging on the steady periodic amplitude. In the former case, the impulse response sets the relevant time and length scales, while in the latter the periodic response dominates, and between these both are important.

III. HEAT TRANSFER ANALYSIS

Equations (4) and (5) are valid for any LTI system. The example of exponential decay is useful as a simple means of showing the circumstances under which accumulation becomes important and how it connects the impulse response to the periodic response. Now, we replace the exponential decay with the thermal response of a multilayered sample heated and probed by Gaussian laser spots, including both the cross-plane and in-plane thermal conductivities of each layer.

Thermal conduction through layered structures in isotropic media has been described in several places,[13,16] and Cahill[11] gave a specific solution for TTR. Here we adopt the approach described by Carslaw and Jaegar[13] for one-dimensional conduction and extend it to account for radial, anisotropic effects using a Hankel transformation.[5]

For a single slab of material in the frequency domain, the temperature, θ_t, and heat flux, f_t, on the top side of the slab are related to the temperature, θ_b, and heat flux, f_b on the bottom side through[13]

$$\begin{bmatrix} \theta_b \\ f_b \end{bmatrix} = \begin{bmatrix} \cosh(qd) & \frac{-1}{\sigma_z q}\sinh(qd) \\ -\sigma_z q \sinh(qd) & \cosh(qd) \end{bmatrix} \begin{bmatrix} \theta_t \\ f_t \end{bmatrix}. \tag{10}$$

Here d is the layer thickness, σ_z the cross-plane thermal conductivity, and $q^2=i\omega/\alpha$, where α is the thermal diffusivity. Multiple layers are handled by multiplying the matrices for individual layers together,

$$\begin{bmatrix} \theta_b \\ f_b \end{bmatrix} = \mathbf{M}_n \mathbf{M}_{n-1} \cdots \mathbf{M}_1 = \begin{bmatrix} A & B \\ C & D \end{bmatrix} \begin{bmatrix} \theta_t \\ f_t \end{bmatrix}, \tag{11}$$

where $\mathbf{M}_n$ is the matrix for the bottom layer. An interface conductance G is treated by taking the limit as the heat capacity of a layer approaches zero and choosing σ_z and d such that $G=\sigma_z/d$. If the bottom surface of the nth layer is assumed to be adiabatic, or if the nth layer is treated as semi-infinite, then in both cases Eq. (11) reduces to $C\theta_t+Df_t=0$ and the surface temperature will be given by

$$\theta_t = \frac{-D}{C} f_t, \tag{12}$$

where f_t is the heat flux boundary condition applied to the top surface. In the majority of our experiments, the semi-infinite boundary condition is an accurate description of the physical situation.

Equation (12) can be conveniently extended to include the effects of radial conduction with a zero-order Hankel transform.[11,13] Applying the transform to the diffusion equation in cylindrical coordinates and repeating the procedure described in Eqs. (10)–(12) yields an identical result, except that now q in Eq. (10) is given by

$$q^2 = \frac{\sigma_r k^2 + \rho c i\omega}{\sigma_z}, \tag{13}$$

where σ_r and σ_z are the radial, or in-plane, and cross-plane thermal conductivities, respectively, ρ is the density of the layer, c_p is the specific heat, and k is the transform variable. The heat flux term f at the boundary is given by the Hankel

transform of a Gaussian spot with power A_0 and $1/e^2$ radius w_0. The surface temperature from Eq. (12) then becomes

$$f = \left(\frac{-D}{C}\right)\frac{A_0}{2\pi}\exp\left(\frac{-k^2 w_0^2}{8}\right). \tag{14}$$

The frequency response H in real space is found by taking the inverse Hankel transform and then weighing the result by the probe intensity distribution, which is taken as a Gaussian spot with $1/e^2$ radius w_1,[11]

$$H(\omega) = \frac{A_0}{2\pi}\int_0^\infty k\left(\frac{-D}{C}\right)\exp\left(\frac{-k^2(w_0^2+w_1^2)}{8}\right)dk, \tag{15}$$

where w_0 and w_1 are the pump and probe $1/e^2$ radii, respectively. This solution for the frequency response is inserted into Eq. (5), which is solved numerically. In practice, an upper limit of integration in Eq. (15) on the order of $10/\sqrt{w_0^2+w_1^2}$ is sufficient for the integral to converge, although if both radii become less than ~ 5 μm this value may need to be increased.

The case where the two beam spots are offset may also be used to study thermal transport. Li *et al.*[17] used this geometry and a numerical simulation to determine the thermal properties of multilayer thin films by varying the frequency of modulated continuous-wave beams. Here we extend Eq. (15) to obtain an analytical solution for the case where the pump spot is separated by a distance x_0 from the probe spot in the Cartesian plain. In this case, some of the symmetry is lost and $H(\omega)$ is given by

$$H(\omega) = \left(\frac{2}{\pi w_1^2}\right)\int_{-\infty}^{\infty}\int_0^\infty \theta\left(\sqrt{(x-x_0)^2+y^2}\right) \times \exp\left(\frac{-2(x^2+y^2)}{w_1^2}\right)dydx, \tag{16}$$

where $\theta(\sqrt{(x-x_0)^2+y^2}) = \theta(r)$ is given by

$$\theta(r) = \int_0^\infty kJ_0(kr)\left(\frac{-D}{C}\right)\left(\frac{A_0}{2\pi}\right)\exp\left(\frac{-k^2 w_0^2}{8}\right)dk, \tag{17}$$

and J_0 is a zero-order Bessel function of the first kind. While Eq. (16) is not as convenient to evaluate as Eq. (15), it is still tractable numerically. In our TTR implementation, we have found that sensitivity to radial transport is of similar order for offset spots compared to aligned spots. However, alignment of offset beam spots is somewhat more challenging than coaxial spots because the offset, which is typically on the order of microns, must be accurately determined. In the case of aligned spots, optimal overlap is indicated when the signal is maximized.

IV. SENSITIVITY TO RADIAL TRANSPORT

The one-dimensional, single-pulse solutions for a 100 nm layer of Al on two substrates, Si and SiO_2, are plotted in Fig. 4 over 12.5 ns, the time between pulses from the Ti:sapphire oscillator. Silicon has a relatively high thermal conductivity, 148 W/m K at room temperature, while the conductivity of SiO_2 is two orders of magnitude lower, $\sim$1.4 W/m K. In both cases, but especially for SiO_2, the response clearly does not decay to zero before the next pulse arrives. Therefore, accumulation effects will be important. The solution will take on aspects of the steady periodic response, and the associated thermal length scale, $L \sim \sqrt{2\alpha/\omega_0}$, compared to the spot size will determine the sensitivity of the solution to radial transport.

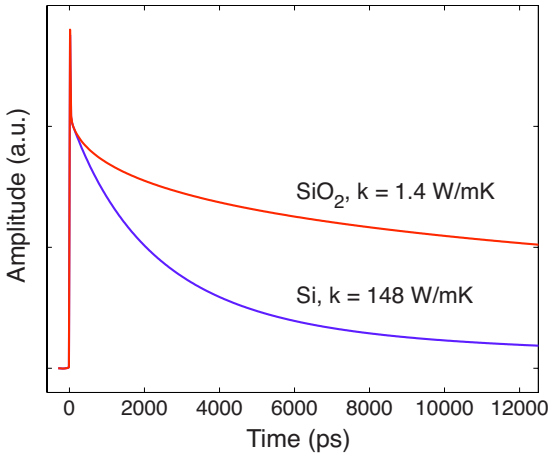

FIG. 4. (Color online) The one-dimensional single-pulse solutions for a 100 nm layer of Al on two substrates, Si and SiO_2, over 12.5 ns, the time between pulses from the Ti:sapphire oscillator.

We use a multidimensional least-squares minimization routine to vary the physical parameters of interest to match the output of the lock-in amplifier to Eq. (5). Either the amplitude or phase data can be compared to Eq. (5) for fitting. In practice, we find that fitting to the phase produces more reliable results because it is slightly less noisy and removes any difficulties associated with normalization. This approach is similar to fitting to the ratio of in-phase and out-of-phase components of the lock-in signal.[18] Fitting the phase does introduce the problem of determining the true phase of the thermal signal with respect to the lock-in reference wave. The signal cables, EOM, and photodiode all have their own response, which collectively can be represented by the transfer function Z_{inst}, such that for a given input $\exp(i\omega t)$ the output will be given by

$$A_{\text{inst}}\exp(i\omega t + \phi_{\text{inst}}) = Z_{\text{inst}}\exp(i\omega t), \tag{18}$$

where ϕ_{inst} is the phase delay introduced by the instrumentation. Thus to fit the phase data, we need a way to determine ϕ_{inst} and subtract it from the measured phase. One way to do this is to split off a small fraction of the modulated pump beam and measure its phase directly with the detector. A second method, which we employ, is to make use of the fact that the out-of-phase, or imaginary, part of Eq. (5) should be constant as the delay time crosses $\tau=0$.[11] After the data are collected, the change in the out-of-phase signal, ΔY_0, and in-phase signal, ΔX_0, are noted as the delay time crosses $\tau=0$. From this the phase introduced by the instrumentation is computed from $\Delta\phi=\tan^{-1}(\Delta Y_0/\Delta X_0)$ and is subtracted from the measured signal.[18]

To quantify the sensitivity of the signal to radial conduction, we define the phase sensitivity to a parameter x in a manner similar to that of Gundrum *et al.*:[7]

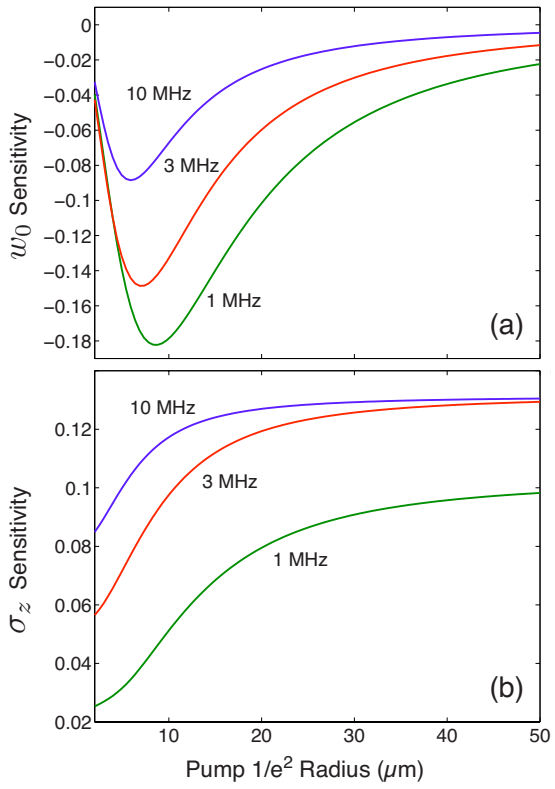

FIG. 5. (Color online) (a) Sensitivity of the signal to the pump spot radius at three frequencies for a sample of SiO_2 coated with 100 nm of Al, plotted as a function of the pump spot radius. (b) Sensitivity of the signal to the cross-plane thermal conductivity of the SiO_2 under the same conditions.

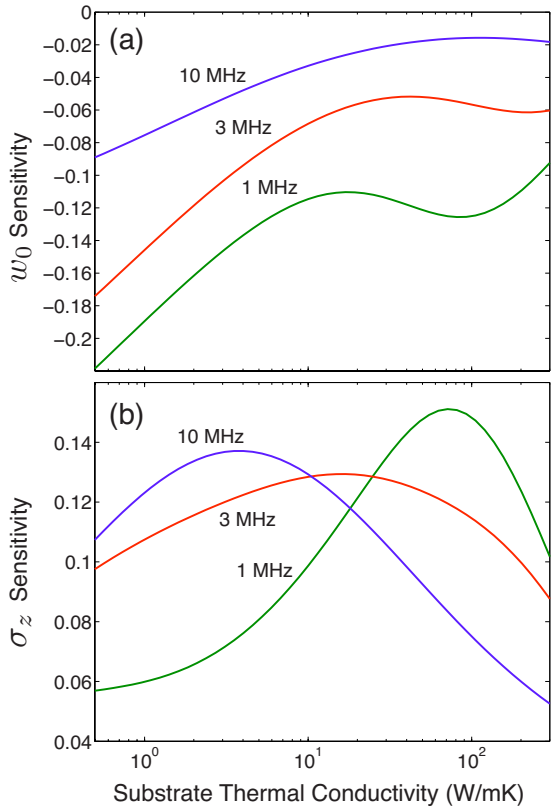

FIG. 6. (Color online) (a) Sensitivity of the signal to the pump spot radius at three frequencies for a sample coated with 100 nm of Al, now plotted as a function of the sample thermal conductivity. The pump radius is fixed at 10 μm and the probe radius is 5 μm. Sensitivity to radial transport increases with decreasing substrate thermal conductivity due to stronger accumulation effects. (b) Sensitivity of the signal to the cross-plane thermal conductivity of the substrate under the same conditions.

$$S_x = \frac{d\phi}{d \ln x}, \tag{19}$$

where the phase, ϕ, is in radians.

Figure 5(a) shows the sensitivity to the pump $1/e^2$ radius, S_{w_0}, plotted as a function of w_0. The substrate is SiO_2 and the probe $1/e^2$ radius, w_1, is fixed at 5 μm. The values are plotted for a delay time, τ, of 1000 ps, although the curves look similar over the range of delay times. The sensitivity is shown at 3 modulation frequencies: 1, 3, and 10 MHz. As expected, at lower frequencies the signal is more sensitive to spot size since the thermal length scale, $L \sim \sqrt{2\alpha/\omega_0}$, increases with decreasing frequency. As a function of spot size, sensitivity is maximized when the pump and probe spots are of similar order.

To put these curves into perspective, the sensitivity to the cross-plane thermal conductivity, a typical parameter of interest, is plotted for the same sample under the same conditions in Fig. 5(b). At 1 MHz when the beam spots are of the same order, the signal is approximately four times more sensitive to spot size than thermal conductivity (i.e., a 5% error is spot size leads to an error up to 20% in the thermal conductivity fit). On the other hand, using a pump spot $1/e^2$ radius of 25 μm and a modulation frequency of 10 MHz, the measurement is 25 times more sensitive to cross-plane thermal conductivity than spot size, and in addition, the relative uncertainty associated with measuring a beam spot with a 25 μm radius is small. Therefore, for basic cross-plane thermal conductivity measurements, a large pump spot and a high modulation frequency are the best combination to reduce uncertainties due to beam spot geometry. There are situations where small beam spots are desirable, for example, to increase the fluence at the sample surface, or for high-resolution spatial thermal conductivity mapping.[4] In these cases, even at high frequency, the sensitivity to spot geometry can be a significant fraction of the sensitivity to thermal conductivity, and care should be taken to accurately characterize the beam spots.

An interesting and somewhat counterintuitive aspect of the sensitivity to radial transport is that it increases with decreasing substrate thermal conductivity. One might expect that lateral heat spreading would be more of an issue when the substrate thermal conductivity is higher. However, as we show in Fig. 3(b), when the thermal decay of a single pulse is long compared to the laser pulse period, stronger accumulation effects cause the signal to approach the steady periodic solution, and the associated periodic length scale plays a more dominant part. In Fig. 4, we show the single-pulse response for SiO_2 and Si, and clearly the thermal decay in the SiO_2 sample is much slower compared to the pulse time. Thus, the measured signal [Eq. (5)] will have a stronger dependence on the periodic thermal length scale, $L \sim \sqrt{2\alpha/\omega_0}$.

The spot sensitivity is plotted as a function of the substrate thermal conductivity in Fig. 6(a). The pump radius is fixed at 10 μm and the probe radius is 5 μm, and again the

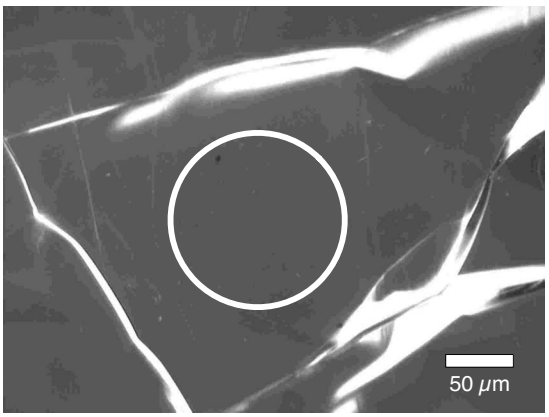

FIG. 7. An image of our HOPG sample coated with 72 nm of Al. Large grains are clearly visible. The pump and probe spots are focused within the white circle in the image.

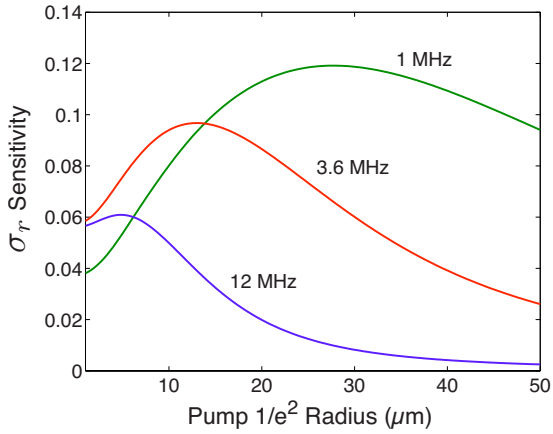

FIG. 8. (Color online) Sensitivity of the signal from HOPG to in-plane thermal conductivity. The delay time is fixed at $\tau=1000$ ps and the probe $1/e^2$ radius is fixed at 5 μm, while the pump radius is varied.

delay time is fixed at 1000 ps. As we expect, the magnitude of the sensitivity increases at lower substrate thermal conductivities and increases with decreasing modulation frequency. The sensitivity to cross-plane thermal conductivity under the same conditions is shown in Fig. 6(b) for reference.

V. ANISOTROPIC MEASUREMENTS: HOPG

We have examined the interplay between pulse accumulation and radial conduction and have shown how it affects the sensitivity of the measured signal to spot geometry. In most cases, the goal is to minimize the dependence of a cross-plane thermal conductivity measurement on the spot conditions. In this case, a high modulation frequency is the best choice.

It is also possible to vary the modulation frequency and spot size to isolate the thermal conductivity in different directions. A measurement at high modulation frequency and with a large spot size can be used to eliminate radial transport and to extract the cross-plane thermal conductivity and the thermal interface conductance between the metal transducer layer and the substrate. Then, a second measurement can be made with a smaller spot size and a lower modulation frequency. In this regime, radial effects become import and the measurement may be sufficiently sensitive to in-plane transport to extract the in-plane thermal conductivity.

We demonstrate the technique with HOPG. It is highly anisotropic and its thermal properties are well known, so it is a convenient benchmark. HOPG has a lamellar structure, composed of stacked planes. The bonding forces within the lateral planes are much stronger than those between the planes, explaining its highly anisotropic elasticity and lattice thermal conductivity.[19] It is also characterized by large single-crystal regions which can be expected to exhibit maximum mechanical and thermal anisotropies. Literature values for the cross-plane thermal conductivity are on the order of 5–8 W/m K, while the in-plane thermal conductivity is around 2000 W/m K, or 300 times higher than the cross-plane value.[20] Figure 7 shows an image of a HOPG sample from our charge coupled device camera. The large grains are clearly visible. The sample has been coated with 72 nm of Al, which serves as the thermal transducer. The pump and probe spots were focused within the white circle in the image.

The details of our experimental setup have been given elsewhere.[5] Unlike other TTR systems described in literature, our pump beam is frequency doubled to 400 nm. This also allows us to use a coaxial geometry where the pump and probe beams go through the center of the same objective lens onto the sample, simplifying alignment, and producing undistorted Gaussian spots. Dielectric mirrors and color filters isolate the pump beam from the detector, allowing us to measure relatively rough samples since the filters are not affected by scattering of the pump beam into different polarizations and angles. A pair of lenses focuses the pump beam onto the doubling crystal and recollimates it; by adjusting the distance between the lenses, we change the divergence of the beam and therefore can easily change the size of the focused pump spot on the sample from radii between 4 and 50 μm.

In Fig. 8, the sensitivity of HOPG to the in-plane thermal conductivity, σ_r, is plotted as a function of pump spot size. All calculations use the best-fit values for thermal properties, as listed in Table I. The delay time is fixed at $\tau=1000$ ps and the probe $1/e^2$ radius is held constant at 5 μm while the pump radius is varied. At 12 MHz modulation and when the pump radius is 50 μm, there is virtually no sensitivity to σ_r. At lower frequencies and smaller pump spot sizes, however, the measurement becomes sensitive to radial conductivity.

Figure 9 shows both the phase and amplitude data, along with best-fit curves, at a modulation frequency of 11.6 MHz, a probe radius of 5 μm, and a pump radius of 50 μm. Under these conditions, the measurement is insensitive to the in-plane conductivity and we find the cross-plane thermal

TABLE I. Results for HOPG at 300 K.

Property	$\omega_0/2\pi$ (MHz)	Radius (μm)	Measured (W/m K)	Literature (W/m K)
σ_z	11.65	50	6.1	5.7
σ_r	3.65	27	1983	1950
σ_r	1.11	27	2080	1950

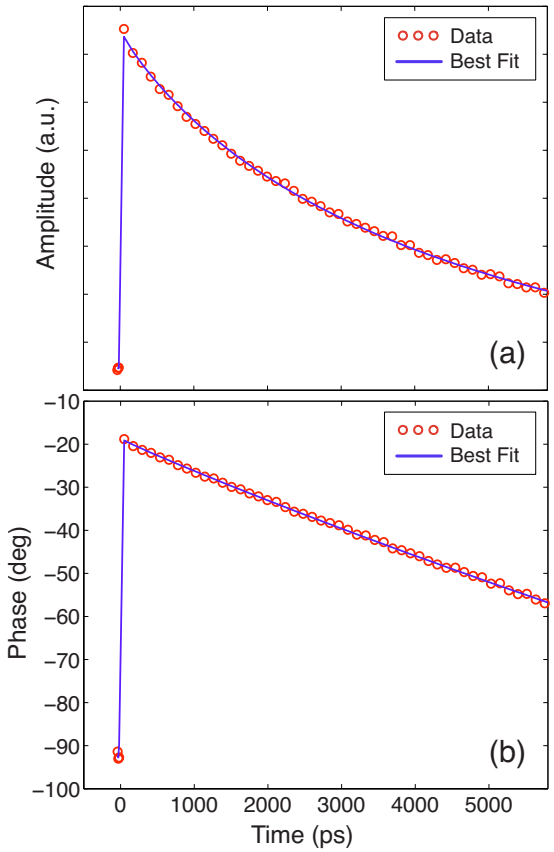

FIG. 9. (Color online) Phase and amplitude data for HOPG, along with best-fit curves for cross-plane thermal conductivity, at a modulation frequency of 11.6 MHz, a probe radius of 5 μm, and a pump radius of 50 μm. In this regime, in-plane transport is not a factor.

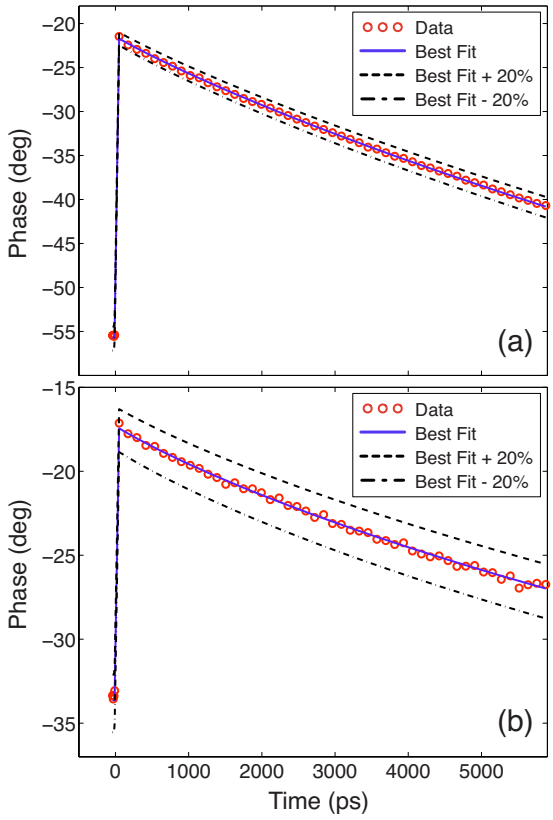

FIG. 10. (Color online) HOPG phase data and best-fit curves for in-plane thermal conductivity, σ_r, at 3.6 MHz (a) and 1 MHz (b). Solutions obtained by varying σ_r by $\pm 20\%$ are also shown.

conductivity, σ_z, to be 6.1 W/m K and the Al-HOPG thermal interface conductance, G, to be 50 MW/m^2 K. The density and specific heat of HOPG were taken as 2700 kg/m^3 and 709 J/kg K, respectively.[20]

Following this measurement, the pump spot radius was reduced to approximately 27 μm and the measurement was repeated at two lower frequencies: 3.65 and 1.11 MHz. From the sensitivity analysis shown in Fig. 8, with a 27 μm pump radius we expect the measurement to be somewhat sensitive to σ_r at 3.65 MHz and more sensitive at 1.11 MHz. In Fig. 10, we plot the phase data and best-fit curves at both frequencies and also the solutions obtained by varying σ_r by $\pm 20\%$. The cross-plane conductivity and interface conductance values are taken from the high frequency measurement shown in Fig. 9, while the in-plane thermal conductivity was varied to match the data. Measurements were repeated at multiple fluence levels to ensure that the sample was not perturbed beyond the linear regime.

The thermal conductivity of HOPG depends somewhat on the sample quality and preparation, but typical room-temperature values for the in-plane thermal conductivity are on the order of 2000 W/m K.[20] The best-fit value obtained for the in-plane thermal conductivity at 3.6 MHz is 1983 W/m K, within 2% of the room-temperature literature value. At 1.11 MHz the value is 2080 W/m K, around 5% higher than the 3.6 MHz measurement. This discrepancy most likely comes from small nonidealities in spot geometry, such as slightly elliptical beam spots, which would become more of a factor at lower frequencies. There is also more noise in the 1.11 MHz signal due to increased $1/f$ noise in the laser power. The results for HOPG are summarized in Table I.

VI. SUMMARY

Accumulation effects from a high repetition-rate pulse source such as a Ti:sapphire oscillator are an important factor in thermal measurements because for the majority of materials, the response due to one pulse does not fully decay before the next pulse arrives. While this complicates the interpretation of the measured signal, it also makes the technique more powerful by essentially probing two length scales simultaneously. With a clear understanding of this behavior, one can minimize the impact of spot geometry on a thermal measurement, or appropriately manipulate the modulation frequency and spot size to rapidly extract both cross-plane and in-plane thermal properties of a sample with two measurements.

ACKNOWLEDGMENTS

The authors would like to thank Professor David Cahill and Xuan Zheng of the University of Illinois at Urbana-Champaign for their many helpful discussions, and Xiaoting Jia for providing HOPG samples. This work was supported by NSF Grant No. CTS-0506830, DTRA Grant No. HDTRA1-07-1-0015, and DoD and NSF Graduate Research Fellowships for A. J. Schmidt.

[1] C. A. Paddock and G. L. Eesley, J. Appl. Phys. **60**, 285 (1986).
[2] W. S. Capinski, H. J. Maris, T. Ruf, M. Cardona, K. Ploog, and D. S. Katzer, Phys. Rev. B **59**, 8105 (1999).
[3] P. M. Norris, A. P. Caffrey, R. J. Stevens, J. M. Klopf, J. James, T. McLeskey, and A. N. Smith, Rev. Sci. Instrum. **74**, 400 (2003).
[4] S. Huxtable, D. G. Cahill, V. Fauconnier, J. O. White, and J.-C. Zhao, Nature Mater. **3**, 298 (2004).
[5] A. Schmidt, M. Chiesa, X. Chen, and G. Chen, Rev. Sci. Instrum. **79**, 064902 (2008).
[6] R. J. Stoner and H. J. Maris, Phys. Rev. B **48**, 16373 (1993).
[7] B. C. Gundrum, D. G. Cahill, and R. S. Averback, Phys. Rev. B **72**, 245426 (2005).
[8] K. E. O'Hara, X. Hu, and D. G. Cahill, J. Appl. Phys. **90**, 4852 (2001).
[9] E. MacCormack, A. Mandelis, M. Munidasa, B. Farahbakhsh, and H. Sang, Int. J. Thermophys. **18**, 221 (1997).
[10] W. S. Capinski and H. J. Maris, Rev. Sci. Instrum. **67**, 2720 (1996).
[11] D. G. Cahill, Rev. Sci. Instrum. **75**, 5119 (2004).
[12] D. G. Cahill, K. Goodson, and A. Majumdar, J. Heat Transfer **124**, 223 (2002).
[13] H. S. Carslaw and J. C. Jaeger, *Conduction of Heat in Solids* (Oxford University Press, New York, 1959).
[14] A. V. Oppenheim, A. S. Willsky, and S. Hamid Nawab, *Signals and Systems*, 2nd ed. (Prentice-Hall, Englewood Cliffs, NJ, 1996).
[15] *User's Manual, Model SR844 RF Lock-In Amplifier*, 2.6 ed. (Stanford Research Systems, Sunnyvale, CA, 2003).
[16] A. Feldman, High Temp. - High Press. **31**, 293 (1999).
[17] B. Li, L. Pottier, J. P. Roger, D. Fournier, and E. Welsch, Rev. Sci. Instrum. **71**, 2154 (2000).
[18] R. M. Costescu, M. A. Wall, and D. G. Cahill, Phys. Rev. B **67**, 054302 (2003).
[19] R. Nicklow, N. Wakabayashi, and H. G. Smith, Phys. Rev. B **5**, 4951 (1972).
[20] *CRC Handbook of Chemistry and Physics*, 87th ed., edited by D. R. Lide (Taylor & Francis, Boca Raton, FL, 2007).